Jurnal Tribologi 47 (2025) 1-23

MYTRIBOS Malaysian Tribology Society

Jurnal Tribologi

Website : jurnaltribologi.mytribos.org e-issn: 2289-7232

Wear rate prediction of hybrid composites: A comparative study using experimental analysis, finite element simulation and machine learning prediction

Ravitej Y P [1*], Keshavamurthy R [2], Rahul Kumar [1], Krantikumar Kshaurad [3], Balachandra Halemani [4], Ramakumar B V N [5], Sripad Kulkarni S [5], Ramesh Shankaranarayana [6]

[1] Department of Mechanical Engineering, Dayananda Sagar University, INDIA.
[2] Department of Mechanical and Automobile Engineering, CHRIST University, Bengaluru 560074, Karnataka, INDIA.
[3] Department of Mechanical Engineering, Dayananda Sagar College of Engineering, INDIA.
[4] Department of Mechanical Engineering, KLE Technological University, INDIA.
[5] Department of Aerospace Engineering, Dayananda Sagar University, INDIA.
[6] College of Engineering and technology, University of technology and applied sciences - Nizwa, Sultanate of Oman.
*Corresponding author: ravitejyp@gmail.com

KEYWORDS

Finite element analysis
Residual analysis
Correlation matrix
Polynomial regression

ABSTRACT

This study evaluates wear rate predictions by comparing experimental results with Finite Element Analysis (FEA) simulations, focusing on the influence of track radius. Regression models were developed to analyze the trends, while residual analysis identified deviations between the two approaches. A correlation matrix highlighted significant relationships between wear rate, pressure, and sliding distance. Confidence interval analysis confirmed the reliability of both models, though polynomial regression provided a more accurate representation of wear rate trends than linear models. While FEA predictions are closely aligned with experimental data, some discrepancies suggest the need for further refinement in computational modeling to improve accuracy. Future work will focus on enhancing FEA simulations and expanding experimental validation for better predictive reliability.

Received 7 April 2025; received in revised form 6 May 2025; accepted 22 July 2025.
To cite this article: Ravitej et al. (2025). Wear rate prediction of hybrid composites: A comparative study using experimental analysis, finite element simulation and machine learning prediction. Jurnal Tribologi 47, pp.1-23.

1.0 INTRODUCTION

Transformation of materials to different application is the cup of tea in today's generation. High strain materials, Alloy steels , Additive manufacturing materials plays a vital role[1], [2], [3]. Composite materials research helps in discovery on new materials[4] that include polymer matrix[5], metal matrix composites[6] for various applications[7]. Use of Biofuels[8] and Bio fiber is the emerging field in the sustainable manufacturing process. In fabrication of composites mould design plays a vital role[9]. In the context of this study, hybrid composites refer to aluminum matrix composites reinforced with a combination of ceramic (Zircon)[10] and solid lubricant (Graphite) particles. The purpose of hybridization is to enhance the mechanical and tribological properties beyond what is achievable with a single reinforcement. Silicon carbide contributes significantly to hardness and load-bearing capacity, thereby improving wear resistance under high contact stresses. Graphite, being a solid lubricant, reduces friction at the sliding interface by forming a transfer layer, leading to lower wear rates and smoother sliding behavior. This synergistic combination allows the composite to withstand severe operating conditions while minimizing material loss. The study demonstrates that hybrid composites exhibit superior performance compared to mono-reinforced counterparts, particularly in reducing the wear track radius and friction coefficient under dry sliding conditions[11].

The distribution, size, and interaction of these reinforcements within the aluminum matrix are critical in determining the overall tribological response. Hence, hybrid composites offer an optimized balance of strength and lubrication, making them suitable for high-performance applications in tribological systems. The precise distribution of force and strain in a pin can be computed using finite element analysis (FEA)[12], which is useful in many industrial applications. Aluminium MMC tribological layers of wear can be studied with the pin-on-disc equipment under various loads and at a constant sliding speed[13]. Archard's wear equation and constant pressure from finite element modeling can also be used to determine the wear depth[14]. Pin deterioration starts at the borders and moves inward.FEA simulation software[15]. The coefficient of wear, and constant pressure on the pin can all be simulated with ANSYS. With a finer nodal mesh and higher accuracy, the FEA numerical solutions compute more slowly[16]. It is possible to do a pin-on-disc experiment's thermal analysis using coated and uncoated discs, which exhibit the desired thermal characteristics[17]. Finite element analysis using microstructure-based analysis can solve issues with regular geometry-shaped particle hybrid metal matrix composites[9].

The study of the electrical contact resistance of materials can be aided by creating a friction model that predicts adhesive wear and pin contact for plastically deformed asperities[18]. We can employ continuous adaptive re-meshing to eliminate the elemental distortion brought on by deformation in the finite element numerical model[19]. Thermo-plasticity, heat transmission across the contact interface, and surface evolution to wear can all be ascertained using the numerical model [20]. Additionally, it provides the link between wear rate, disc speed, and transition temperatures[6]. Elastoplastic finite element analysis shows strain and force on the disc and pins under various friction situations when applied to the pin-on-disc tests[21]. It demonstrates how the Von-Mises force and plastic strain both rise with friction[22].

It is possible to create an asymptotic model that will produce equations for evaluating contact wear parameters and determining the wear scar patterns of two contacting surfaces[23].While finite element software models require a large amount of processing time, the asymptotic model is simpler and just as accurate[18]. A 2D cell model that is based on the actual microstructure can be made to investigate the substantial plastic deformation at high temperatures. The findings of the pin and disc experiment, which is conducted on various metals and validated by FEM, indicate

that aluminum alloy has a lower wear percentage [22], low coefficient of friction, low contact pressure, etc. Touch of experiment, FEA and Statistical analysis is a rare combination for composite. This paper describes the essence of all these and also gives the insight of mechanism undergone with the wear and simulation and its comparative study.

2.0 METHODOLOGY

2.1 Experimental Procedure

Stir casting is selected for the fabrication of composite due to its homogenius mixing of reinforcements in molten matrix. Intitally reinforcemetns are preheated to the 200 degree Celcius to remove moisture content. Copper chills are placed at one end of the mould to get uniform solidification of the molten composite. Chill end properties of the solid composite is charecterized. Zircon reinforcement are added at the Wt.% of 3,6,9,12. The dry sliding wear test is conducted on these specimens with the boundry conditions as shown in table 1. Schematic diagram of pin on Disc is shown in the figure 1.

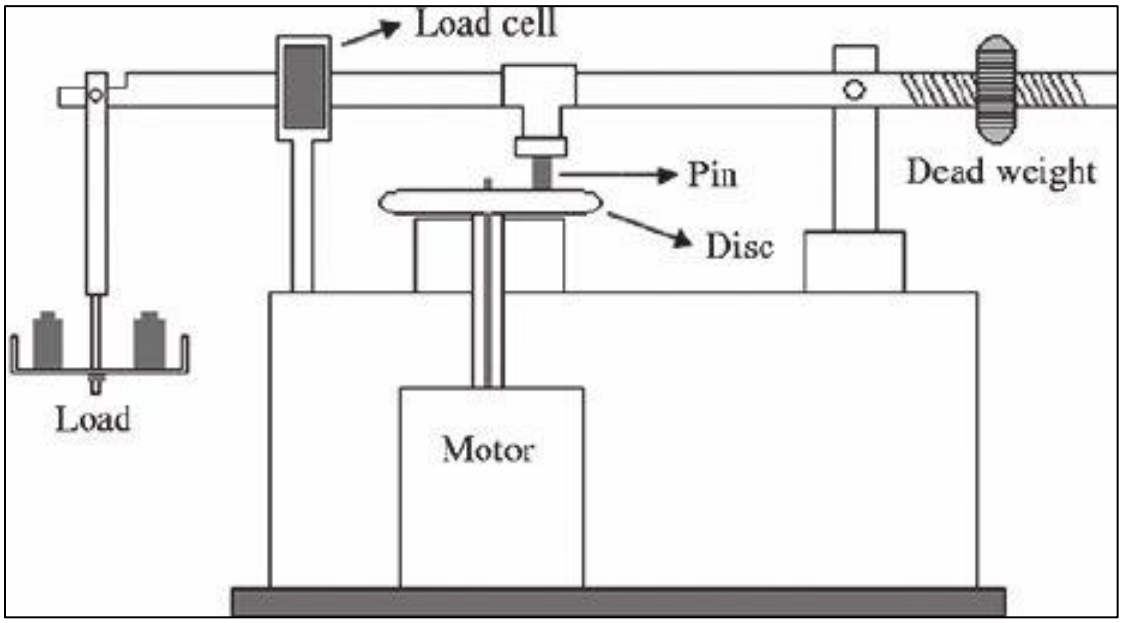

Figure 1 : Pin On Disc apparatus[24].

2.2 FEA Modelling

The ANSYS workstation is used for numerical simulations. The disc measures 250 mm in radius and 5 mm in thickness 22 mm in height and 8 mm in diameter pin. The disc surface and the pin face make a friction contact during assembly.Pin mechanical properties acquired using various characterizations are supplied to ANSYS by importing the assembly file into ANSYS Workbench environment, as seen in Figure 2. Since the wear on the pin is more concentrated than the wear on the disc, Quadra mesh is used to mesh the assembled model. For the Disc and Pin, the element sizes are 3 mm and 1 mm respectively. Grain refining is carried out at the pin-disc

interface to improve the accuracy of the findings. The meshing model in ANSYS WORKBENCH is displayed in Figure 3.

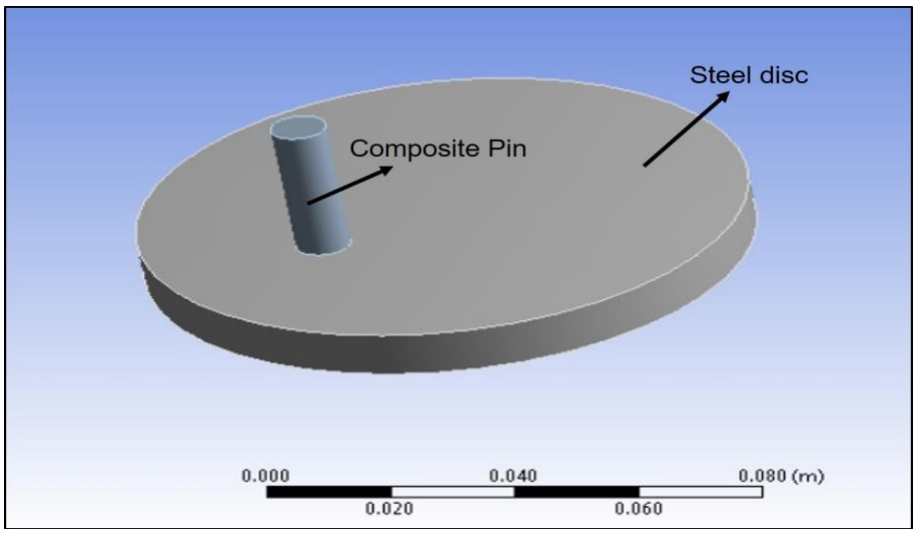

Figure 2: 3D Model of the pin and disc interface.

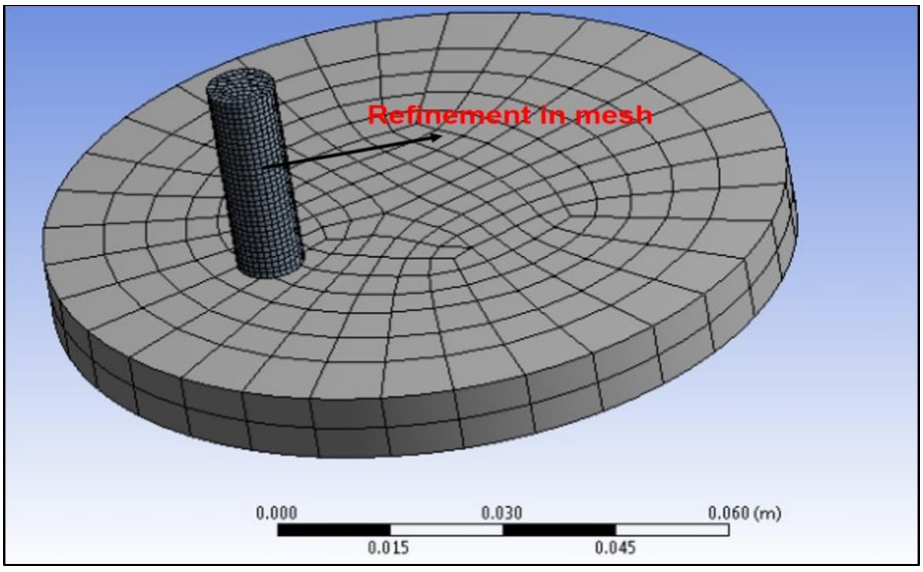

Figure 3: Finite Element Model (Meshed Model).

Between the contact surfaces, a frictional contact is formed. The coefficient of friction is derived from the outcomes of experiments. The boundary condition is implemented on the meshed model, as illustrated in Figure 4 and Table 1, The disc is rotated at varying sliding distance while a load is applied to the pin's top constantly. At the point where the pin and disc make contact, there is progressive wear was observed.

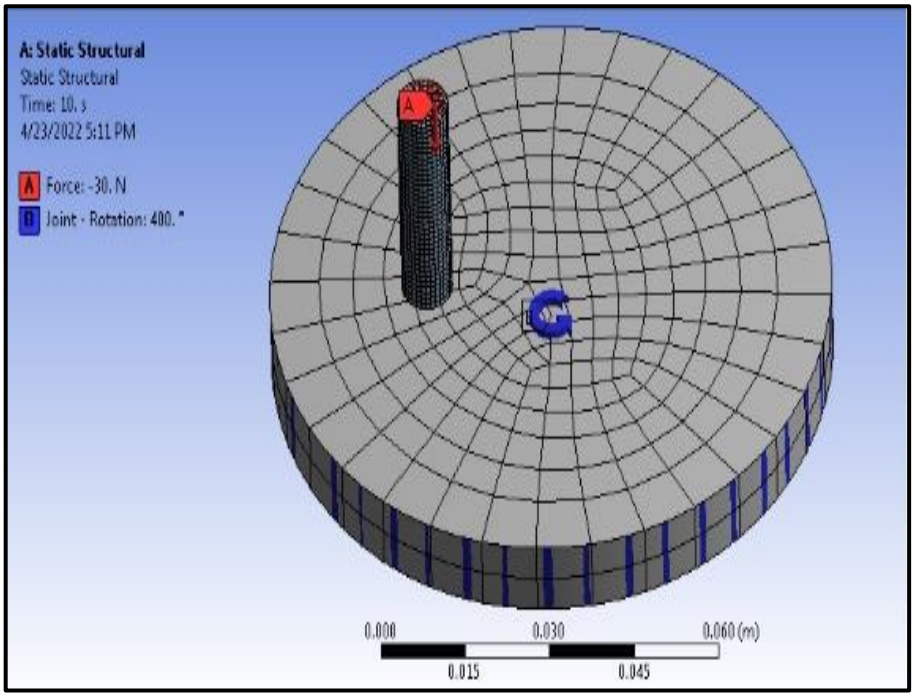

Figure 4: Load and Boundary conditions.

Table 1: Boundary conditions applied to pin on disc.

SL No	Analysis	Parameter 1 (Load, N)	Parameter 2 (Sliding Distance, mm)	Parameter 3 (Speed, rpm)
1	Change in Sliding distance	30	226.08	400
2		30	301.4	400
3		30	376.8	400
4		30	452.16	400
5		30	527.52	400

2.2.1 Calculation of Wear Rate Using FEA

The desired results for the comparison are obtained by the post-solver ANSYS after boundary conditions have been applied to the meshed model. The solution evolves total deformation and wear pressure. The following formula is used to determine the wear coefficient:

Wear coefficient = Wear depth/ (Pressure*sliding distance) …… (1)

Here, The ANSYS workbench solver's greater values of total deformation and pressure are used to calculate wear depth and pressure values. The value specified as the boundary condition is sliding distance. The relationship, as indicated in the equation, yields the wear rate.

Wear Rate = Wear coefficient * Pressure …… (2)

The value derived from the equation is the wear coefficient. When employed as a boundary condition, pressure is the entire load placed on the pin. Thus, wear depth and wear pressure that is acquired from the solver are taken into account while calculating total wear. The findings of the experiment and the wear found by numerical modeling are contrasted. The results' percentage inaccuracy is assessed and recorded.

2.3 Statistical Analysis (ANOVA)

In a wear study, ANOVA (Analysis of Variance) is used to analyze the effects of different factors on material wear, helping to determine whether significant differences exist between tested conditions A One-Way ANOVA can be used if there is only one independent variable, such as different material types, while a Two-Way ANOVA is useful if two factors, like load and speed, are studied simultaneously.

2.4 Regression Analysis

Linear regression and polynomial regression are both statistical methods used to model the relationship between an independent variable and a dependent variable, but they differ in complexity and application. Linear regression assumes a straight-line relationship, where changes in the independent variable result in proportional changes in the dependent variable, It is simple, easy to interpret, and useful when data follows a linear trend. In contrast, polynomial regression extends this concept by incorporating higher-degree terms. Polynomial regression is more flexible and effective when data exhibits a curved trend, but it can lead to overfitting if the degree is too high. While linear regression is ideal for simple relationships like predicting sales based on advertising spend, polynomial regression is useful for more complex patterns, such as modeling the trajectory of an object or analyzing material wear over time. Choosing between the two depends on the nature of the data and the required balance between simplicity and accuracy.

3.0 RESULTS AND DISCUSSION

Since out of different combinations of reinforcements and matrix, 9wt.% of Zircon. Change in Sliding distance are analysed experimentally using Pin on Disc, Finite element simulation and its correlation is measured.

3.1 Experimental Wear Rate Study

Wear rate data serves as direct experimental evidence of wear occurrence in the studied composites, even though the main document lacks detailed discussion or microstructural analysis of wear mechanisms. The wear rates were systematically recorded under controlled tribological conditions (constant load of 30 N, speed of 400 rpm, and varying sliding distances), revealing consistent trends across different zirconia reinforcement levels. Notably, the wear rate decreases significantly with increasing zircon content, with the 12 wt.% composite exhibiting the lowest wear rates, while the as-cast chill end condition shows the highest wear as shown in the table 2.

Table 2: Effect of track radius on wear loss, COF, and wear rate.

Zircon wt.%	(Load, N)	(Speed, rpm)	(Sliding Distance, mm)	Wear rate
12wt.%	30	400	226.08	0.005645
	30	400	301.4	0.005789
	30	400	376.8	0.005969
	30	400	452.16	0.006012
	30	400	527.52	0.006121
9 wt.%	30	400	226.08	0.00346
	30	400	301.4	0.003556
	30	400	376.8	0.003756
	30	400	452.16	0.003987
	30	400	527.52	0.004125
6 wt.%	30	400	226.08	0.00701
	30	400	301.4	0.007123
	30	400	376.8	0.007258
	30	400	452.16	0.007456
	30	400	527.52	0.007512
3 wt.%	30	400	226.08	0.00835
	30	400	301.4	0.008452
	30	400	376.8	0.008658
	30	400	452.16	0.008963
	30	400	527.52	0.009125
As cast chill end	30	400	226.08	0.009571
	30	400	301.4	0.009654
	30	400	376.8	0.009785
	30	400	452.16	0.009958
	30	400	527.52	0.01038

The Figure 5 illustrates the relationship between Wear rate (WR) v/s Track radius (TR) for different chill levels in a casting process. As observed, WR increases with TR across all chill levels, indicating a trend where higher TR values correspond to greater WR. The "As cast chill end" condition consistently exhibits the highest WR values, while the "9% chill" condition shows the lowest WR across all TR values. This suggests that increasing the chill percentage tends to reduce WR, up to a certain point. However, the "6% chill" and "3% chill" conditions display higher WR than "12% chill" and "9% chill," implying that the effect of chill on WR is non-linear. The data highlights that optimal chill percentages can be selected based on the desired WR characteristics, balancing durability and performance in the casting process.

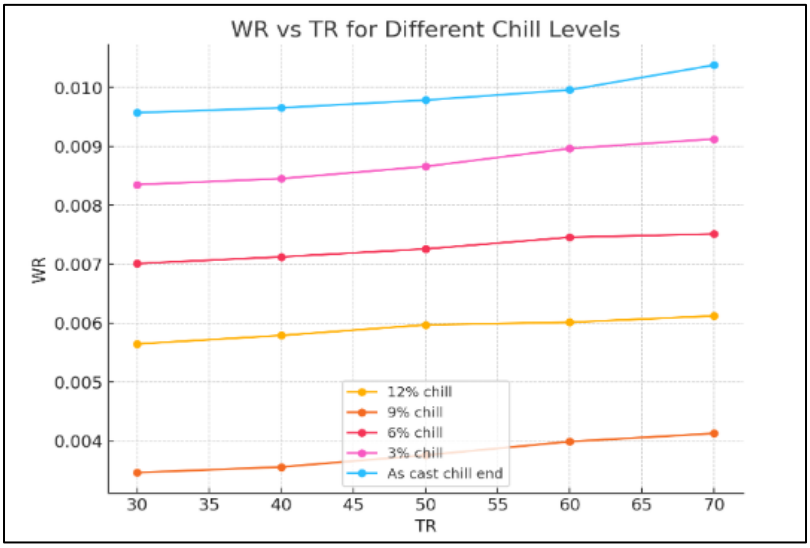

Figure 5: Wear rate (gms) v/s Track radius for different chill levels.

Wear occurrence is evidenced through quantitative measurements of wear rates under controlled tribological testing conditions. The study investigates the effect of varying zirconium (zircon) reinforcement levels ranging from 3 wt.% to 12 wt.% on the wear behavior of the composite material, using a constant load of 30 N and a speed of 400 rpm across different sliding distances. The results clearly show that wear rate decreases with increasing zircon content, indicating enhanced wear resistance due to the presence of hard ceramic particles that likely act as barriers to material removal during sliding. The highest wear rates are observed in the as-cast chill end samples and the composites with lower zircon content (3 wt.%), suggesting poor resistance to wear due to the softer matrix and lack of sufficient reinforcement. In contrast, the 12 wt.% zircon composite exhibits the lowest wear rates, demonstrating that increased reinforcement improves the tribological performance. This trend reflects typical wear mechanisms where harder phases help reduce material loss by limiting plastic deformation and micro-cutting.

The bar chart (figure 6) provides a comparative view of WR across different chill levels for various TR values. It highlights the effect of WR with chill. The "As cast chill end" condition consistently shows the highest WR, indicating the highest material loss or wear. In contrast, "9% chill" exhibits the lowest WR, making it the most effective in minimizing wear. "12% chill" also performs well but has slightly higher WR than "9% chill." Interestingly, WR increases again for "6% chill" and "3% chill,"suggesting that beyond a certain chill percentage, the beneficial effects

start diminishing. Across all conditions, WR increases with TR, indicating a progressive wear effect over time or under higher stress. This comparison reinforces the idea that an optimal chill percentage exists around Wt.9% to achieve the best wear resistance.

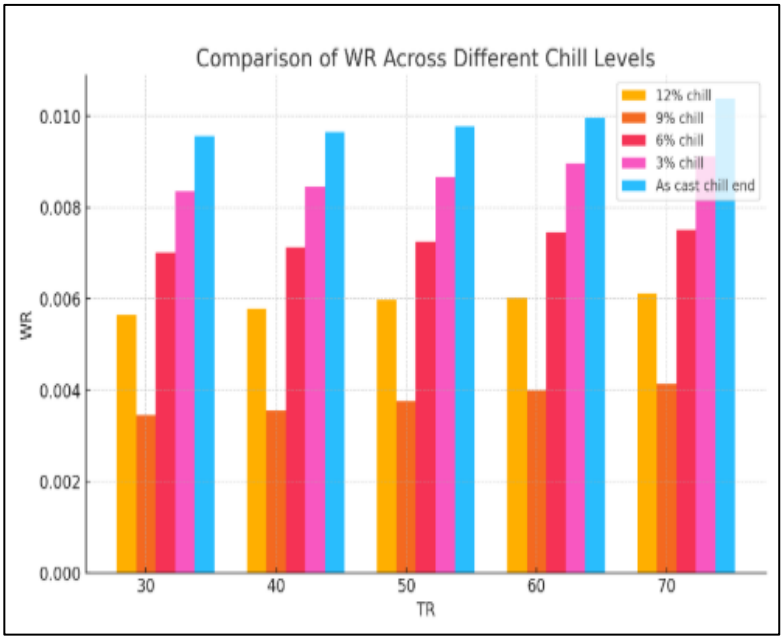

Figure 6: Comparison of Wear rate across different chill levels.

3.2 Statistical Wear Rate Analysis

The statistical analysis confirms a significant relationship between chill levels and WR. The descriptive statistics show that 9% chill has the lowest mean WR (0.003777), making it the most wear-resistant condition, while "As cast chill end" has the highest WR (0.009870), indicating the most wear as shown in figure 7. The standard deviation is lowest for 12% chill (0.000189), suggesting more consistency in WR values, while 3% chill (0.000330) has the highest variability.The ANOVA test resulted in a p-value of 1.39e-18, which is extremely low, indicating a statistically significant difference in WR across the different chill levels. This means the variations observed in WR are not due to random chance but are directly influenced by the chill percentage. Analysis suggests that chill percentage plays a crucial role in wear resistance, with 9% chill providing the optimal balance for minimizing WR shown in table 3.

The correlation analysis reveals a strong to very strong positive relationship between TR and WR across all chill levels. This means that as TR increases, WR also increases significantly. The highest correlation is observed for 9% chill ($r = 0.9923$, $p = 0.0008$), indicating an almost perfect linear relationship between TR and WR. Similarly, 6% chill ($r = 0.9897$) and 3% chill ($r = 0.9881$) also exhibit very strong correlations, reinforcing the trend that WR increases with TR across these conditions. The As cast chill end condition shows the weakest correlation ($r = 0.9479$), though it is still strong and statistically significant ($p = 0.0142$). These results confirm that TR is a major factor influencing WR, regardless of the chill percentage. The slight variations in correlation strength suggest that different chill levels impact the rate at which WR increases, with 9% chill

exhibiting the most consistent trend. This insight can be valuable for optimizing chill levels to minimize WR while maintaining a predictable wear pattern shown in table 3.

Table 3: Statistical analysis (ANOVA).

Chill Level	Count	Mean WR	Std Dev	Min WR	25% WR	Median WR	75% WR	Max WR
12% chill	5	0.0059	0.00018	0.00564	0.00578	0.00596	0.00601	0.00612
9% chill	5	0.0037	0.00028	0.00346	0.00355	0.00375	0.00398	0.00412
6% chill	5	0.0072	0.00021	0.00701	0.00712	0.00725	0.00745	0.00751
3% chill	5	0.0087	0.00033	0.00835	0.00845	0.00865	0.00896	0.00912
As cast chill end	5	0.0098	0.000321	0.009571	0.009654	0.009785	0.009958	0.01038

Table 3: Correlation coefficient study.

Chill Level	Correlation Coefficient (r)	p-value	Strength of Correlation
12% chill	0.9818	0.0029	Very Strong Positive
9% chill	0.9923	0.0008	Very Strong Positive
6% chill	0.9897	0.0013	Very Strong Positive
3% chill	0.9881	0.0016	Very Strong Positive
As cast chill end	0.9479	0.0142	Strong Positive

3.3 Finite Elemental Analysis of Wear Rate

The sliding distance is calculated using Equation 1 and a track radius of 30 mm. With the boundary conditions of sliding distance 226.08mm, constant load 30N, and sliding speed 400 rpm, the wear rate is investigated using ANSYS WORKBENCH. Pressure and total deformation are the desired results of the solution. The wear coefficient and wear rate can be found using the equation. The figure displays the general patterns of deformation and pressure. As seen in Figures 4 and 5, the pin and disc's contact surface experiences the maximum deformation due to its increased force and stress shown in figure 7 and 8. Table 4, shows the comparison of Experimental[6] and FEA wear rate values. It is observed that a minimum Percentage error is observed between the results.

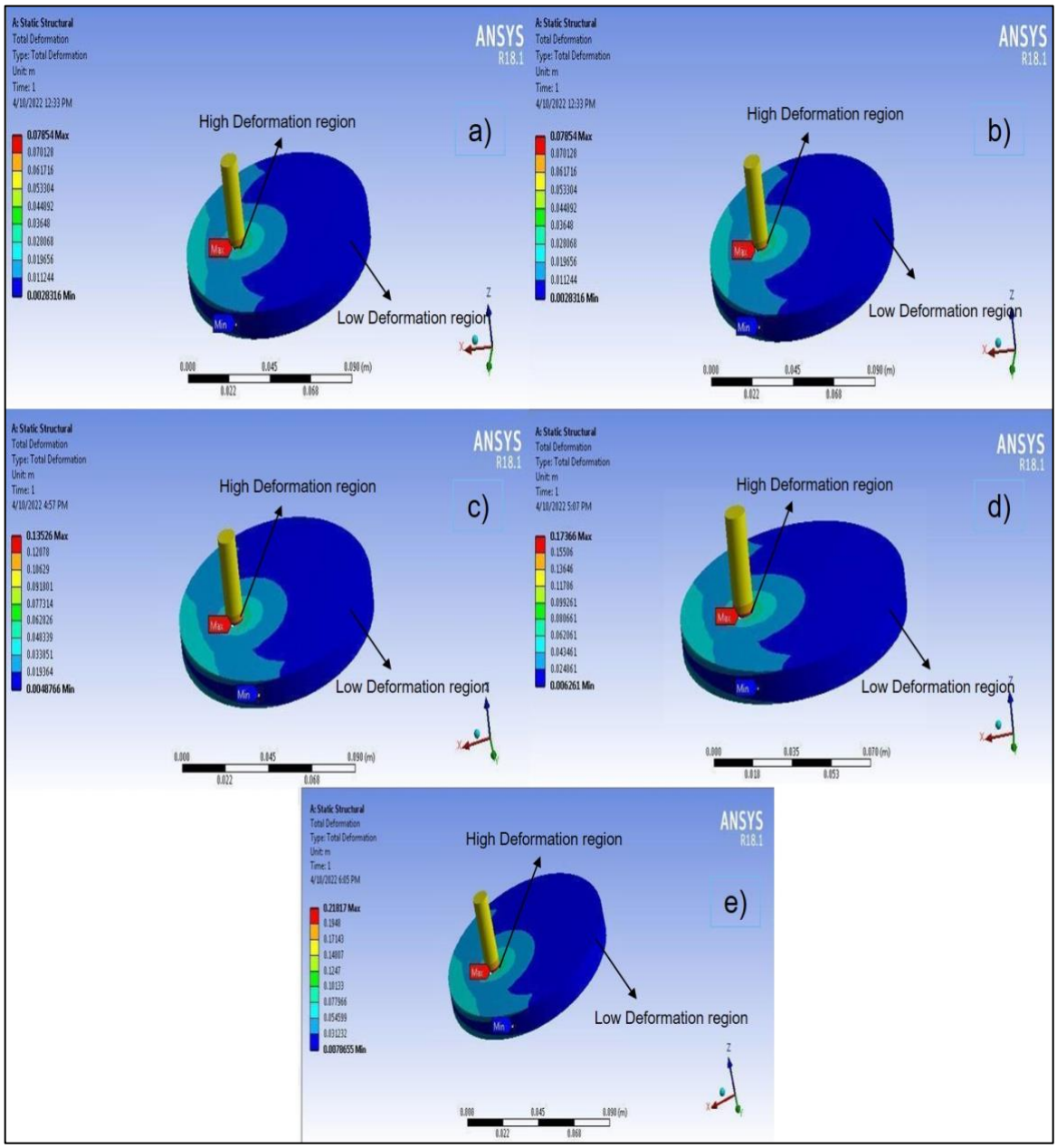

Figure 7: Total deformation V/s (TR (a)30mm, (b) 40mm, (c)50mm, (d)60mm and(e)70mm).

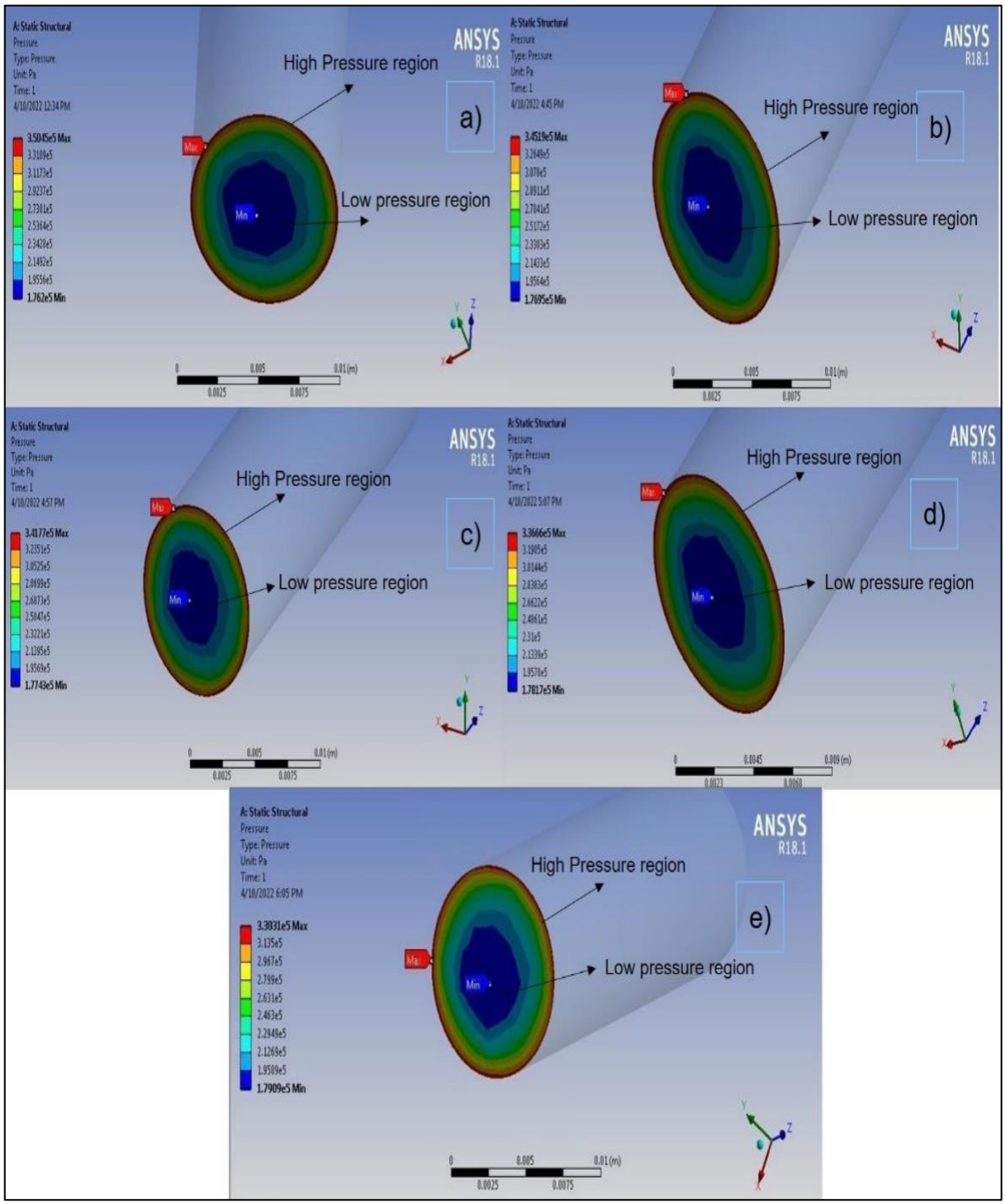

Figure 8: Total Pressure V/s (TR (a)30mm, (b) 40mm, (c)50mm, (d)60mm and (e)70mm).

Table 4: Comparison of wear experimental wear rate and FEA wear rate for SD

Sl.No	TR (mm)	SD (mm)	Wear depth (m)	Pressure (MPa)	Sliding distance (m)	Wear co-efficient max	Wear rate Experimental	Wear rate FEA	% Deviation
			h max	P	S	K*10^{-11}	Q*10^{-3}		
1	30	226.08	0.0785	0.3504	226.08	99.1435	0.00346	0.00347	-0.4
2	40	301.4	0.1090	0.3419	301.4	99.1435	0.00355	0.00361	-1.8
3	50	376.8	0.1352	0.3417	376.8	104.98	0.00375	0.00359	4.4
4	60	452.16	0.1736	0.3366	452.16	114.06	0.00398	0.00384	3.7
5	70	527.52	0.2181	0.3301	527.52	125.24	0.00412	0.00413	-0.3

The Figure 9 compares the wear rates obtained from experimental testing and Finite Element Analysis (FEA) simulations as a function of track radius (mm). The x-axis represents the track radius in millimeters, while the y-axis denotes the wear rate in (Q×10−3). The experimental wear rate is represented by a solid blue line with circular markers, whereas the FEA wear rate is depicted by a dashed red line with square markers. The trend shows that both wear rates increase as the track radius increases. However, there are some discrepancies between the two datasets, particularly in the mid-range of track radius values (around 40–50 mm), where the FEA wear rate deviates slightly from the experimental data. The deviation between the Finite Element Analysis (FEA) results and the experimental track radius values, particularly in the range of 40–50 mm, can be attributed to several key factors. One primary reason is the simplification of material behavior in the FEA model. Real materials often exhibit complex responses such as strain-rate dependence, anisotropy, and microstructural effects, which are difficult to fully replicate in simulations that typically assume idealized elastic or plastic behavior. Frictional interaction also plays a significant role, the coefficient of friction used in the simulation might not accurately reflect the actual conditions during testing due to variables such as surface roughness, temperature, and contamination. Additionally, thermal effects and wear in experiments alter surface properties, which are not considered in most simulations. These discrepancies lead to different stress distributions and deformation patterns.

The Figure 10 illustrates the percentage deviation between experimental and Finite Element Analysis (FEA) wear rates as a function of track radius (mm). The x-axis represents the track radius, while the y-axis denotes the percentage deviation. The green line with triangular markers indicates the deviation across different track radius values. The deviation is relatively small at lower radii (around 30–40 mm), showing slight negative values, meaning the FEA predictions slightly overestimated wear rates compared to experimental data. However, as the track radius increases beyond 40 mm, the deviation rises significantly, peaking above 4% at around 50 mm.

After this peak, the deviation gradually decreases but remains positive until around 70 mm, where it returns closer to zero. This trend suggests that the FEA model provides reasonable agreement with experimental results but exhibits some overestimation at intermediate track radii.

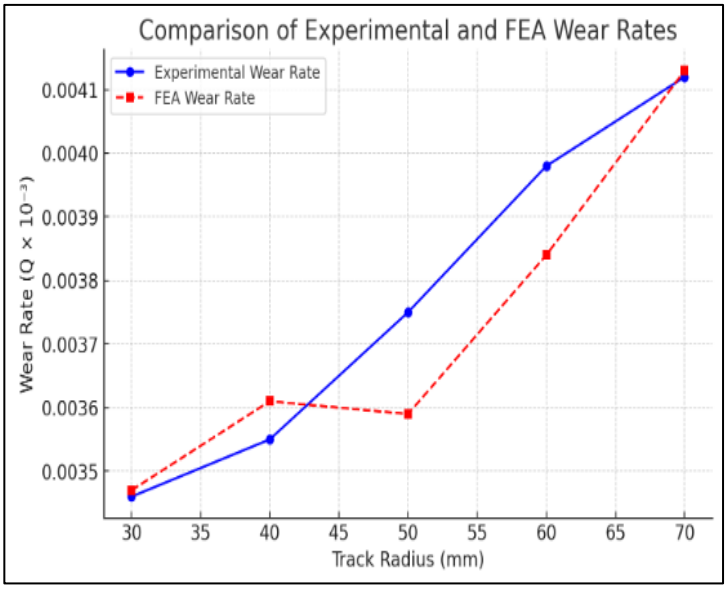

Figure 9: Comparison of Experimental and FEA wear rates.

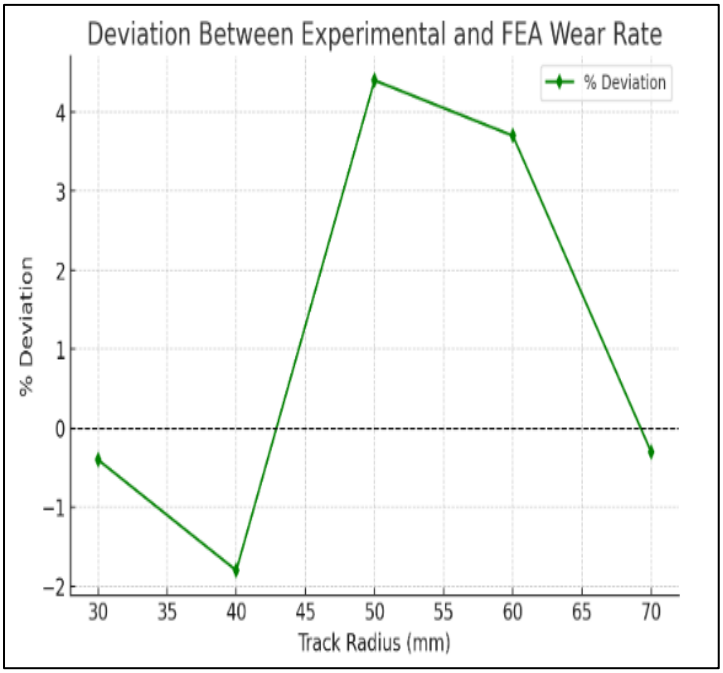

Figure 10: Deviation between Experimental and FEA wear rates.

3.4 Machine Learning Analysis (Regression) And Prediction of Wear rate

The Figure 11, represents a regression analysis of wear rate as a function of track radius, comparing experimental data with Finite Element Analysis (FEA) data. The x-axis represents the track radius (mm), while the y-axis indicates the wear rate ($Q \times 10^{-3}$). The experimental data points are represented by blue circles, whereas the FEA data points are marked by red squares. Two fitted regression lines are included: a solid blue line for the experimental data and a dashed red line for the FEA data. Both fits show a positive linear trend, indicating that wear rate increases with track radius. However, the FEA fit generally predicts lower wear rates than the experimental fit, with noticeable deviations at intermediate values.

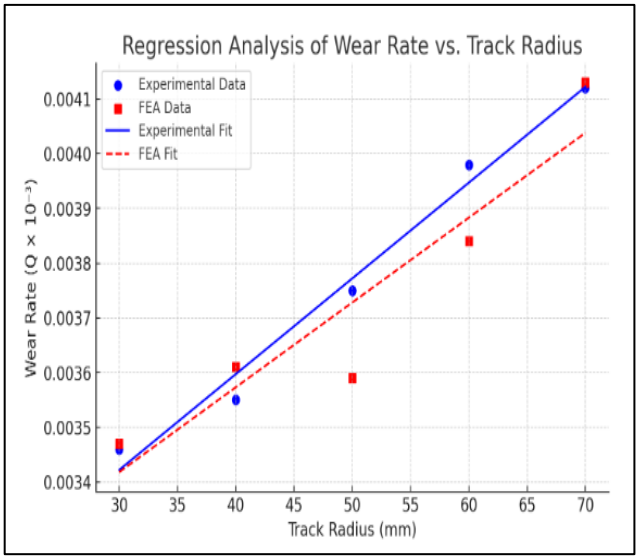

Figure 11: Regression analysis of wear rate v/s Track radius.

The Figure 12 compares linear and polynomial regression models for predicting wear rate as a function of track radius, incorporating both experimental and Finite Element Analysis (FEA) data. The x-axis represents the track radius (mm), while the y-axis denotes the wear rate (Q×10−3). The experimental data points are shown as blue circles, whereas red squares represent the FEA data points. Two types of regression models are depicted: polynomial regression (solid lines) and linear regression (dotted lines). The solid blue and red lines represent polynomial predictions for experimental and FEA data, respectively, while the dotted lines indicate linear regression predictions for both datasets.The polynomial models exhibit a strong upward trend at higher track radii, suggesting a nonlinear relationship between wear rate and track radius. In contrast, the linear models remain nearly flat, failing to capture the increasing trend observed in the data. This discrepancy indicates that a linear regression model may not be sufficient to accurately predict wear rates for larger track radii, whereas a polynomial approach better represents the observed wear behavior. The polynomial regression predictions for both experimental and FEA data suggest that the wear rate increases significantly as the track radius extends beyond the measured data range, emphasizing the nonlinear nature of the wear process.

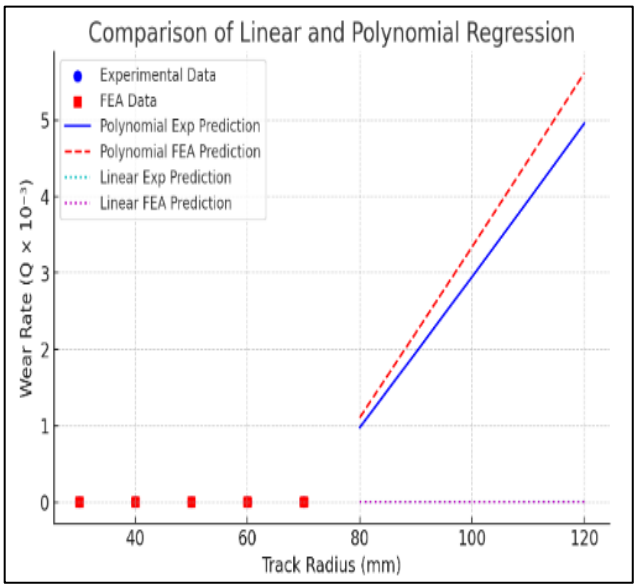

Figure 12: Comparison of Linear and polynomial regression.

Figure 13 displays the residual analysis for the regression of wear rate against track radius, comparing experimental and Finite Element Analysis (FEA) data. The x-axis represents the track radius (mm), while the y-axis shows the residuals, and deviations from the fitted regression lines. Experimental residuals are marked as blue circles, whereas FEA residuals are shown as red squares. The dashed horizontal line at zero represents perfect agreement with the fitted models. Residuals fluctuate both positively and negatively, indicating variations in how well the regression models capture the actual data. The experimental residuals tend to be more evenly distributed around zero, suggesting a relatively balanced fit. On the other hand, the FEA residuals show a wider spread, with some values significantly above or below zero, implying a less accurate fit in certain regions. Notably, the largest deviations for FEA residuals occur at extreme track radius values (around 30 mm and 70 mm). This residual analysis helps assess the accuracy of the regression models and indicates that while both models follow a general trend, discrepancies exist, especially in the FEA predictions.

The correlation matrix visualizes the relationships between different wear-related factors, including track radius (TR), pressure, sliding distance, experimental wear rate (Wear Rate Exp), and Finite Element Analysis (FEA) wear rate (Wear Rate FEA). The color-coded heatmap uses a gradient from blue (negative correlation) to red (positive correlation), with numerical correlation values displayed in each cell.

From Figure 14 (matrix), strong positive correlations are observed between track radius, sliding distance, and wear rates. Specifically, TR and sliding distance have a perfect correlation (1.00), indicating that they increase proportionally. Similarly, wear rate (both experimental and FEA) shows strong positive correlations with TR and sliding distance, confirming that higher track radii and sliding distances lead to increased wear rates.

Conversely, pressure exhibits a strong negative correlation with TR (-0.97), sliding distance (-0.97), and wear rates (-0.94 to -0.96), suggesting that as pressure decreases, wear rate and track radius increase. This inverse relationship is expected in tribological studies where higher

pressures often lead to reduced track radii under constant load conditions.Overall, correlation matrix highlights the key dependencies among wear factors, reinforcing that wear rate is primarily driven by track radius and sliding distance, while pressure plays an inverse role in influencing these parameters.

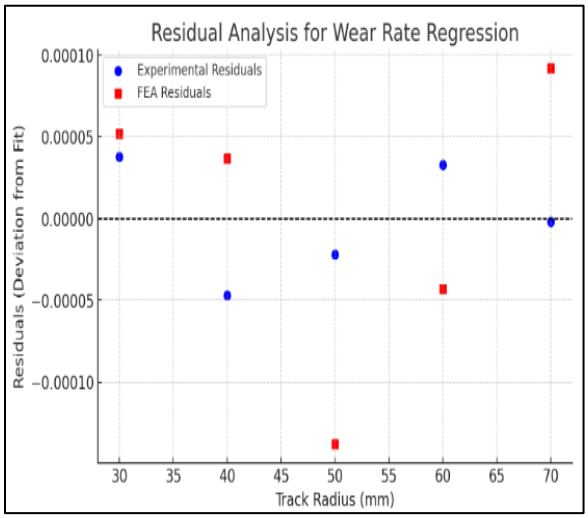

Figure 13: Residual analysis for wear rate regression.

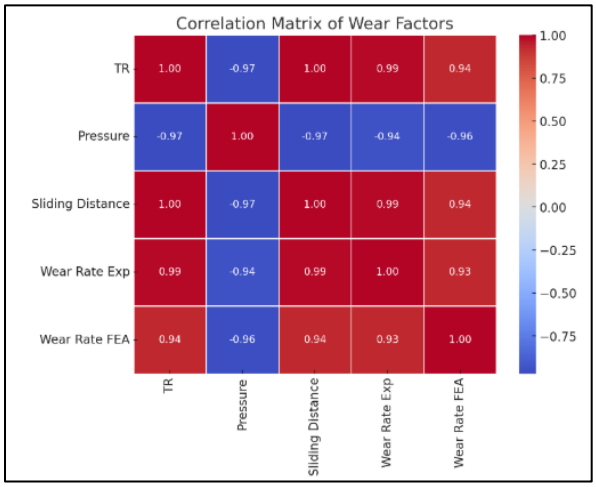

Figure 14: Correlation matrix of wear factors.

Figure 15 illustrates the predicted wear rate for new track radii based on experimental and Finite Element Analysis (FEA) data. The x-axis represents the track radius (mm), while the y-axis shows the wear rate ($Q \times 10^{-3}$). Experimental data points are marked as blue circles, whereas red squares represent FEA data points. The solid blue line represents the predicted wear rate based on the experimental trend, while the dashed red line indicates the FEA-based prediction.The plot includes actual data points up to around 70 mm, with the trend lines extending beyond this range to predict wear rates for larger track radii, up to 120 mm. Both prediction lines exhibit a positive

slope, indicating that the wear rate is expected to increase with the track radius. However, the FEA prediction consistently underestimates the wear rate compared to the experimental prediction, mirroring the trend observed in prior analyses.

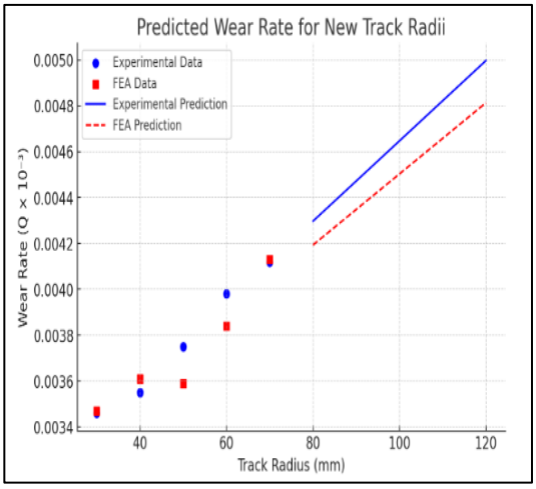

Figure 15: Predicted wear rate for new track radii.

4.0 MICROSTRUCTURAL STUDY

The SEM micrographs presented reveal significant insights into the fracture and wear mechanisms of the developed hybrid aluminum matrix composites. Figures 16(a) and 16 (b) display rough and fragmented surfaces, indicative of brittle fracture behavior and suggesting poor interfacial bonding between the matrix and reinforcement particles. Features such as particle pull-out and microcracks point toward localized debonding and weak load transfer across the interface. In contrast, Figures 16 (c) and 16 (d) exhibit more ductile characteristics, including plastic flow and void coalescence, particularly around spherical or bulbous features likely corresponding to graphite particles. These features confirm the role of graphite as a solid lubricant, contributing to reduced friction and smoother wear surfaces. Figure 16 (e) reveals clustered reinforcement particles, possibly ceramic reinforcements like SiC, surrounded by a relatively smooth matrix interface, suggesting areas of improved wetting and adhesion. Initially, it is observed that matrix and reinforcements are mixed uniformly without any agglomeration, especially at the interfaces of matrix and reinforcements. Figure 16 shows the morphologies of different wt.% of Zircon composites. Wear tracks are observed in 3wt.% of Zircon, delamination of the surface is observed in 6wt.% of Zircon, mild wear is observed at 9wt.% of Zircon and abrasive wear is observed at higher wt.% I, e 12wt.% of Zircon. Since mild wear is observed at 9wt.% of Zircon, the wear rate is minimal at 9wt.% of Zircon. This is due to the Uniform dispersion of reinforcements in the matrix Dislocations are observed at the inter surfaces of the matrix and reinforcements, Tribo layers are formed at the surface for better lubrication properties. But At 12wt.% of Zircon tribolayers are depleted due to higher wt.% of Zircon and promoting oxidation, finally leading to abrasive wear as shown in Figure 16.

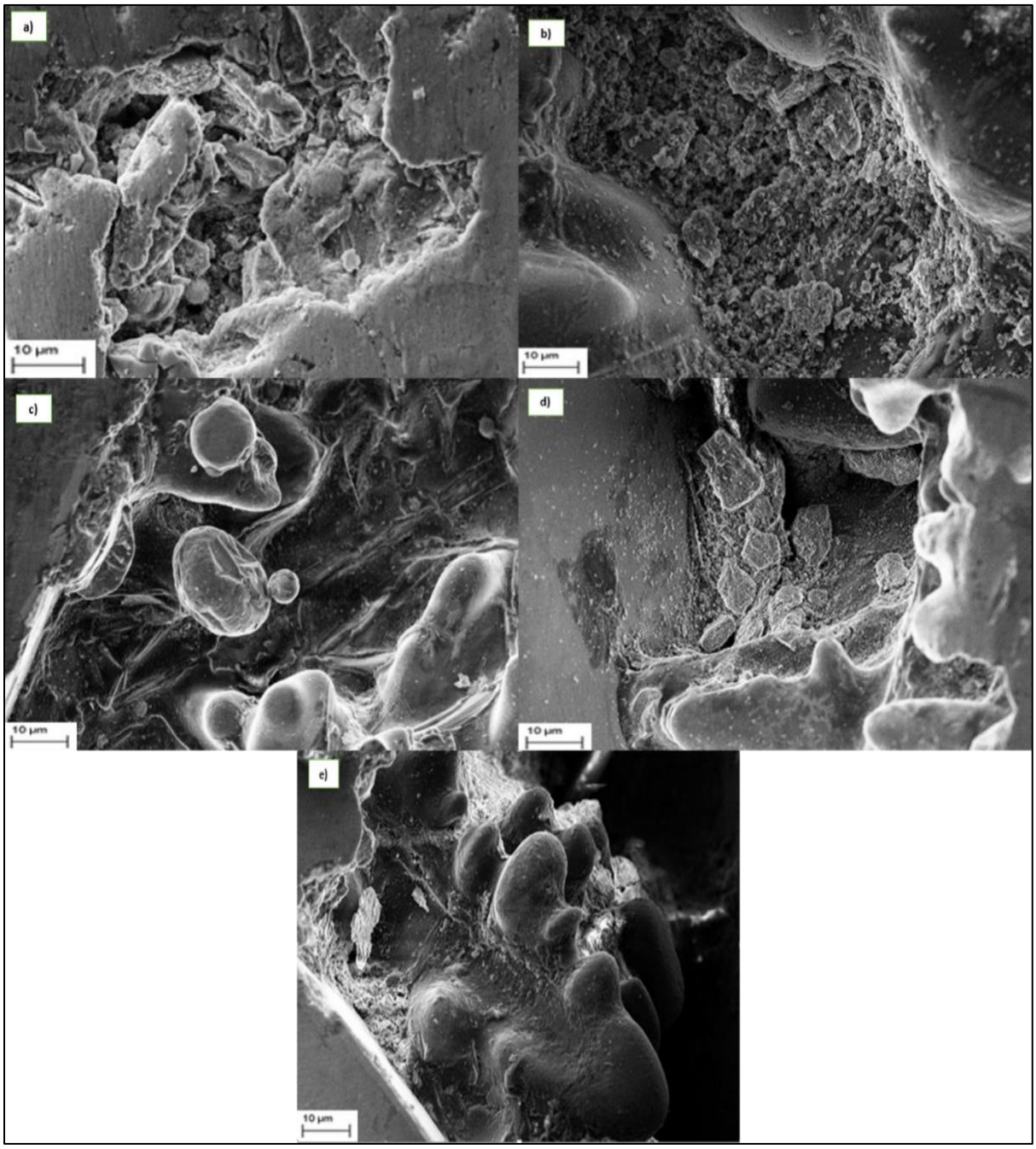

Figure 16: FESEM images of wear tracks of the composite pin after experimentation (0Wt.% Zircon, 3Wt.% Zircon, 6Wt.% Zircon, 9Wt.% Zircon, 12Wt.% Zircon).

5.0 EDX AND ELEMENTAL ANALYSIS

The elemental analysis of the copper chill end is shown in Figure 17 and Table 5 respectively. Since maximum attributes are attained at 9 Wt. % of Zircon and afterward decreases, 9 Wt. % and 12 Wt. % of Zircon are taken into consideration for the investigation. As it is observed that traces of copper are observed at the chill end due to copper chill conserved throughout processing, aluminum is the most promising element in all three cases, while silicon is the second most promising element. When compared to the 12-Wt. % of Zircon, fewer Zircon oxides are generated at 9 Wt. %. Retention of oxygen degrades a material's quality, which leads to pores appearing in the composite material. Therefore, a composite with 9Wt% Zircon has better characteristics than one with 12Wt% Zircon.

Table 5: Elemental analysis of the Copper chill end of (a) As cast, (b) 9Wt.% of Zircon, (c) 12Wt.% of Zircon.

As cast			**9Wt.% of Zircon**			**12Wt.% of Zircon**		
Element	**Weight %**	**Atomic %**	**Element**	**Weight %**	**Atomic %**	**Element**	**Weight %**	**Atomic %**
Al K	81.98	83.57	O K	10.59	16.83	O K	21.69	31.93
Si K	15.76	15.43	Al K	71.41	67.31	Al K	65.08	56.81
Cu L	2.38	1.03	Si K	16.86	15.27	Si K	13.07	10.96
Zircon L	-0.13	-0.04	Cu L	2.26	0.91	Cu L	2.30	0.85
			Zircon L	-1.12	-0.31	Zircon L	-2.14	-0.55
Totals	100.00			100.00			100.00	

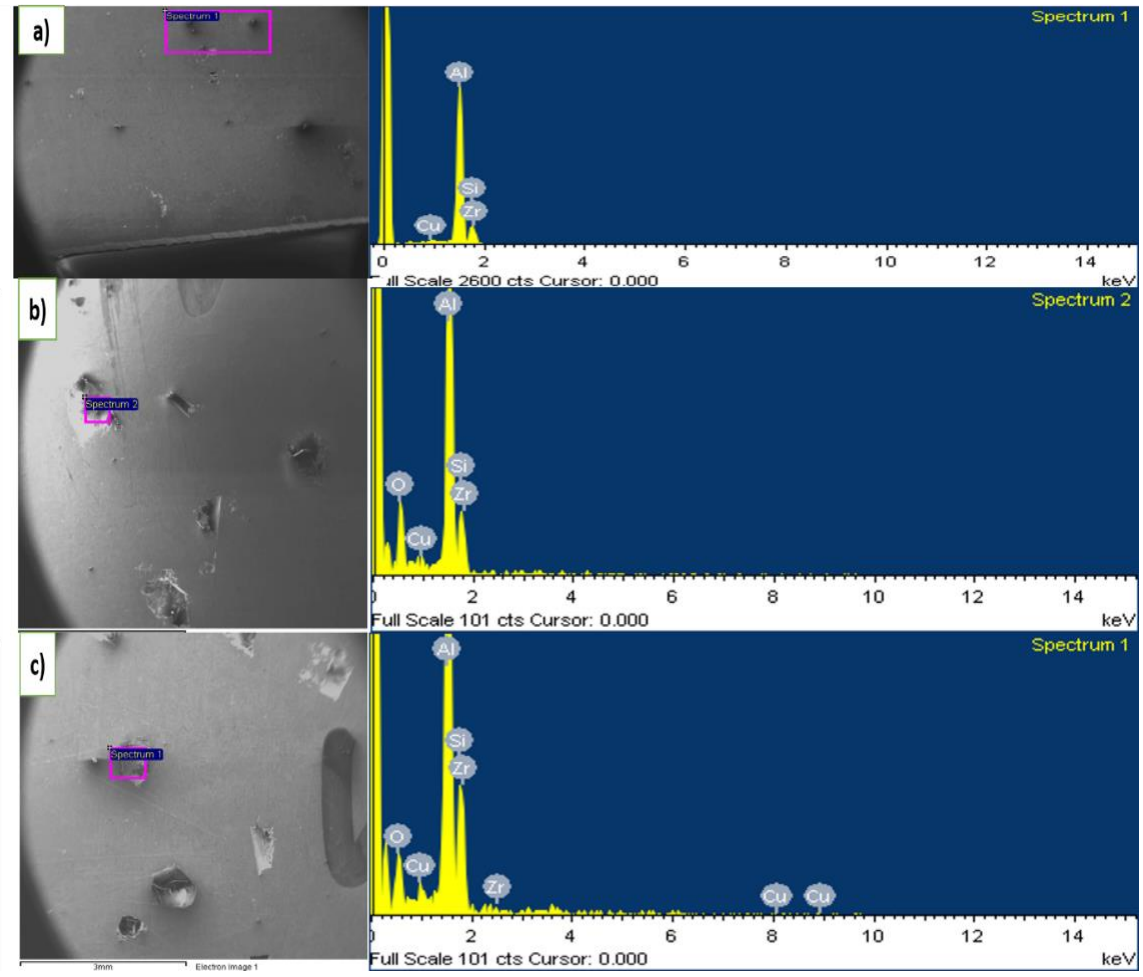

Figure 17: Chill end of a) As cast b) 9Wt.% of Zircon c) 12Wt.% of Zircon.

CONCLUSIONS

This study provides a strong correlation between experimental and Finite Element Analysis (FEA) models in predicting wear rates of hybrid composites. While both approaches provide reliable results, minor deviations at specific track radii suggest the need for further refinement in computational modeling. Regression analysis, particularly polynomial regression, proves to be more effective in capturing the wear rate trends compared to linear models. Residual analysis highlights areas where FEA predictions deviate, reinforcing the importance of model accuracy improvements. The correlation matrix confirms that track radius, sliding distance, and pressure significantly influence wear rates, with polynomial regression offering a better fit for larger track radii. The findings emphasize the necessity of refining FEA simulations and incorporating advanced statistical models for enhanced predictive reliability. Future work will focus on optimizing computational models and expanding experimental validation to improve the accuracy and applicability of wear rate predictions in real-world scenarios.

Data availability statement

The datasets used and analyzed in this study, *"Wear Rate Prediction of Hybrid Composites: A Comparative Study Using Experimental Analysis, Finite Element Simulation, and Machine Learning Prediction,"* are available upon reasonable request from the corresponding author. Due to institutional and confidentiality constraints, the raw data cannot be publicly shared. However, processed data supporting the findings of this study can be made available upon request.

REFERENCES

[1] Song, B., Connelly, K., Korellis, J., Lu, W. Y., & Antoun, B. R. (2009). Improved Kolsky-bar design for mechanical characterisation of materials at high strain rates. *Measurement Science and Technology, 20*(11). https://doi.org/10.1088/0957-0233/20/11/115701

[2] Antoun, B. R., Mac Donald, K., Talamini, B., Stershic, A., Lao, X., & Sandia National Laboratories. (n.d.). *Validation experiments for extensive mechanical deformation of a 304L stainless steel geometry* (pp. 1–3).

[3] Shaw, G., Prorok, B. C., Starman, L. V., & Furlong, C. (2014). *Thermomechanics, infrared imaging, inverse problem methodologies and mechanics of additive advanced manufactured materials (Vol. 7).* Springer. Retrieved from http://www.springer.com/series/8922

[4] Prem Chand, R., et al. (2021). Characterization of banana and e glass fiber reinforced hybrid epoxy composites. *Materials Today: Proceedings, 46*, 9119–9125. https://doi.org/10.1016/j.matpr.2021.05.402

[5] Prem Chand, R., Ravitej, Y. P., Kumar, N., Veerachari, & Gowda, N. A. (2019). Characterization of banana and bagasse fiber reinforced hybrid epoxy composites. *AIP Conference Proceedings, 2057*. https://doi.org/10.1063/1.5085624

[6] Ravitej, Y. P., Mohan, C. B., & Ananthaprasad, M. G. (2022). Dry sliding friction and wear behavior of LM13/zircon/carbon (HMMC's): An experimental, statistical and artificial neural network approach. *Tribology in Industry, 44*(3), 374–393. https://doi.org/10.24874/ti.1223.11.21.03

[7] Maity, D., Siddheshwar, P. G., & Saha, S. (1998). *Advances in fluid mechanics and turbomachinery.* https://doi.org/10.1007/978-3-642-72157-1

[8] Ravitej, Y. P., et al. (2021). Emission characteristics of single cylinder diesel engine with algae oil as biodiesel. *AIP Conference Proceedings, 2316*. https://doi.org/10.1063/5.0036860

[9] Deepak, V., Abhilash, O., Ravitej, Y. P., Veerachari, & Abhinandan, L. (2021). Design and development of progressive tool for mold tag. *AIP Conference Proceedings, 2316*. https://doi.org/10.1063/5.0038385

[10] Ravitej, Y. P., Mohan, C. B., & Prasad, M. G. A. (2021). Corrosion analysis of LM13/ZrSiO4/C hybrid metal matrix composites. *Journal of Corrosion Science and Engineering, 23.*

[11] Sameer, S., & Banda, V. (2018). Bending stresses and wear reduction in an involute spur. *International Journal of Mechanical Engineering and Technology, 5*(3), 432–436.

[12] Sandeep, D., et al. (2021). CFD simulation of transonic turbulent flow past NACA 0012 aerofoil. *AIP Conference Proceedings, 2316.* https://doi.org/10.1063/5.0036890

[13] Ravitej, Y. P., Chandra, B. T., Adarsha, H., Chandrashekar, A., & P. C. R. (2024). Analysis of wear parameters of chill casted LM13/zircon/carbon hybrid composites using experimental and statistical approach. In *Proceedings* (pp. 77–88). https://doi.org/10.52209/2706-977X

[14] Prakash, R. Y., Boganarasimhaiah, M. C., & Gangadharaiah, A. P. M. (2021). Fabrication, micro structural and mechanical characterization of zircon particles (ZrSiO4) reinforced aluminum alloy (MMCs). *Indian Journal of Engineering & Materials Sciences, 28*(6), 549–553. https://doi.org/10.56042/ijems.v28i6.40173

[15] Ravitej, Y. P., Mohan, C. B., & Ananthaprasad, M. G. (2022). Evaluation of copper chill on tribological behaviour of LM13/ZrSiO4/C hybrid metal matrix composites. *Journal of Mines, Metals & Fuels, 69*(12A), 142. https://doi.org/10.18311/jmmf/2021/30143

[16] Prem Chand, R., Halemani, B. S., Chandrasekhar, K. M., Ravitej, Y. P., Raju, T. H., & Udayshankar, S. (2021). Investigation and analysis for mechanical properties of banana and E glass fiber reinforced hybrid epoxy composites. *Materials Today: Proceedings.* https://doi.org/10.1016/j.matpr.2021.05.044

[17] Naveen Kumar, S., et al. (2021). Fabrication and characterization of hardness and microstructure of large sized Al2014–SiC composite. *Materials Today: Proceedings.* https://doi.org/10.1016/j.matpr.2021.05.398

[18] Ravitej, Y. P., Swaroop, V., Ramesh, S., Adarsha, H., Veerachari, & Nischith. (2018). Finite element analysis of mild steel–rubber sandwich composite material. *IOP Conference Series: Materials Science and Engineering, 376*(1). https://doi.org/10.1088/1757-899X/376/1/012040

[19] Ravitej, Y. P., Sandhya, R., & Nandeeshaiah, B. M. (2016). Stress analysis of aero engine spur gear. *International Journal of Innovative Research in Science, Engineering and Technology,* 797–802. https://doi.org/10.15680/IJIRSET.2016.0505632

[20] Prem Chand, R., Halemani, B. S., Chandrasekhar, K. M., Ravitej, Y. P., Raju, T. H., & Udayshankar, S. (2021). Investigation and analysis for mechanical properties of banana and E glass fiber reinforced hybrid epoxy composites. *Materials Today: Proceedings, 47*, 2509–2515. https://doi.org/10.1016/j.matpr.2021.05.044

[21] Naveen Kumar, S., et al. (2021). Fabrication and characterization of hardness and microstructure of large-sized Al2014–SiC composite. *Materials Today: Proceedings, 46*, 9102–9106. https://doi.org/10.1016/j.matpr.2021.05.398

[22] Ravitej, Y. P., Keshavamurthy, R., Adarsha, H., Kumar, V. V., Bavan, D. S., & Asdaque, P. M. G. B. (2025). Effect of zircon on aluminum/graphite alloy hybrid composite and wear characterization with load: Experimental and ANN test. *Journal of Bio- and Tribo-Corrosion, 11*(1), 1–13. https://doi.org/10.1007/s40735-025-00944-7

[23] Ravitej, Y. P., Mohan, C. B., & Ananthaprasad, M. G. (2021). Effect of reinforcement and copper chill on LM13/ZrSiO4/C hybrid metal matrix composites (HMMCs): An experimental and statistical analysis. *China's Refractories, 30*(4), 12–18. https://doi.org/10.19691/j.cnki.1004-4493.2021.04.003

[24] Yusof, S. N. A., Manap, A., Afandi, N. M., Salim, M., & Misran, H. (2015). Mechanical and wear properties of aluminum coating prepared by cold spraying. *AIP Conference Proceedings, 1669*. https://doi.org/10.1063/1.4919182